


Grid voltage sensorless control of a single-phase shunt hybrid active power filter

Mohammad-Sadegh Karbasforooshan¹ | Mohammad Monfared^{1,2} 

¹Department of Electrical Engineering, Faculty of Engineering, Ferdowsi University of Mashhad, Mashhad, Iran

²Department of Electronic and Electrical Engineering, Faculty of Science and Engineering, Swansea University, Swansea, UK

Correspondence

Mohammad Monfared, Department of Electronic and Electrical, Engineering, Faculty of Science and Engineering, Swansea University, Swansea, UK.
Email: mohammad.monfared@swansea.ac.uk

Abstract

Here, a grid voltage sensorless control of an LCL-filtered LC-tuned single-phase shunt hybrid active power filter (HAPF) is proposed, which offers high-quality harmonic current compensation with low hardware requirements. An estimation algorithm replaces the grid voltage sensor and associated circuitry to reduce the size and cost. This paper presents a straightforward and accurate modelling of the suggested structure and its filtering characteristics, followed by a comprehensive yet simple parameter design procedure. An inherent damping technique that uses digital delay rather than virtual or physical damping resistors eliminates the need for additional sensors or extra power losses. As part of the design, a high-quality reference current is generated for the filter, which is then effectively tracked using a proportional controller with sufficient bandwidth and stability margin. An experimental prototype is implemented to verify the theoretical results, and several steady-state and transient waveforms are reported to demonstrate the superior performance of the HAPF.

1 | INTRODUCTION

Harmonic currents generated by non-linear loads cause power quality problems, power losses, stability challenges, unpredictable behaviour of power protection systems, and electromagnetic interferences. Power factor correction and the elimination of current harmonics are mainly achieved using passive power filters (PPFs). While these filters have simplicity and low-cost advantages, parallel resonance with the electric distribution network poses a significant risk. Rather, active power filters (APFs) offer flexibility, quick response, and the ability to fully compensate for harmonics and reactive components [1–5]. Despite the many advantages of APFs, like other power electronic circuits, they have serious restrictions in high-power applications, where power semiconductor switches must be able to handle high voltages and currents. Shunt hybrid active power filters (HAPFs) are regarded as a viable solution in high powers to obtain a balance between the cost and filtering performance. These filters have the advantages of a lower DC-link voltage, higher power handling capability and the possibility of implementation in higher voltage networks [6–8]. Although the DC-link voltage of the converter significantly decreases, the

converter current is still high (due to the series connection of PPF and APF). Recently, a combination of a thyristor-controlled reactor (TCR) with an APF is introduced [9–11]. This structure is the same as the conventional HAPFs, but a TCR is added in parallel with the PPF capacitor to flexibly compensate for the reactive power at the price of added complexity and cost.

Different switching noise filters are used in the HAPF structures. The L filter [6–8], LC filter [12, 13] and LCL filter [14, 15] are used as switching noise filters at the output of the converter of HAPFs. Authors in [15] propose the non-linear modelling and control of a photovoltaic-fed improved three-phase shunt HAPF. By successful use of an LCL filter in their topology, the overall filter size and dimensions are reduced. The dynamic model is obtained in the synchronous reference frame and a non-linear sliding-mode controller is proposed. The passive LCL filter resonance damping is done using a resistor in the capacitor branch at the cost of added losses [15]. The LCL topology provides better switching noise mitigation with a lower total inductance value. However, an exact system modelling and straightforward parameter design procedure for the HAPF applications cannot be found in the literature. Also, the inherent resonance caused by the LCL filter can lead to instability of

This is an open access article under the terms of the [Creative Commons Attribution](https://creativecommons.org/licenses/by/4.0/) License, which permits use, distribution and reproduction in any medium, provided the original work is properly cited.

© 2024 The Authors. *IET Power Electronics* published by John Wiley & Sons Ltd on behalf of The Institution of Engineering and Technology.

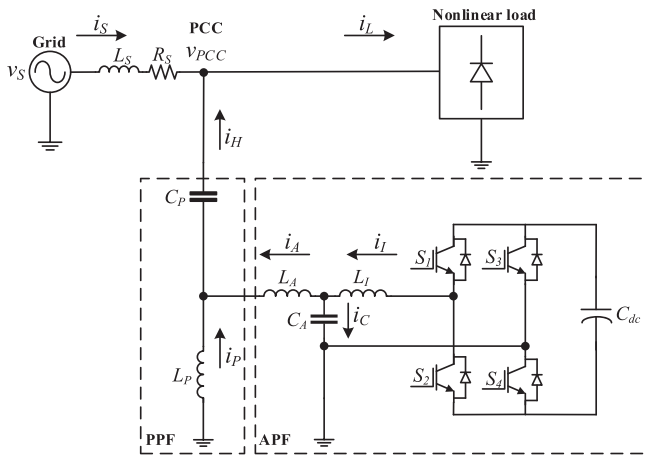


FIGURE 1 LCL-filtered LC-tuned single-phase shunt HAPF.

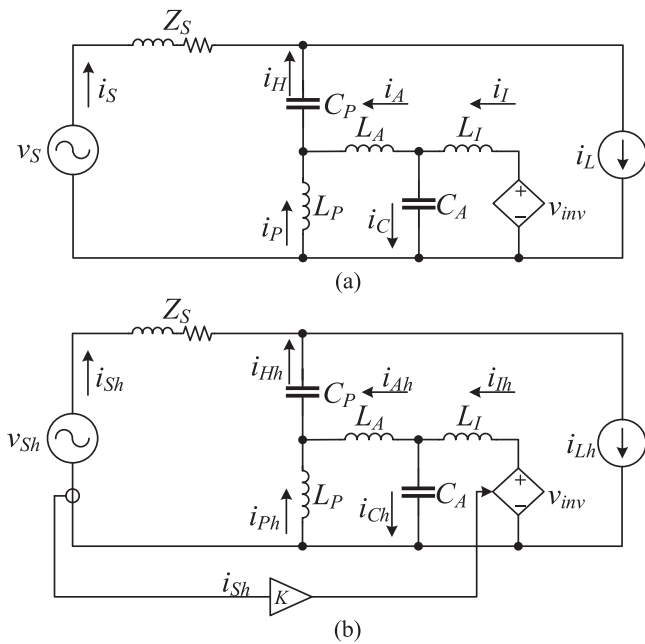


FIGURE 2 Equivalent circuit of Figure 1: (a) for fundamental and (b) harmonic components.

the current control system. Passive and active damping methods are presented to overcome this problem, which add a real or virtual resistor in the filter structure or the control algorithm, respectively. Despite their simplicity, passive damping methods suffer from additional power losses and lower attenuation of switching noises [16, 17]. Active damping methods have the advantages of flexibility and no power losses but have their limitations, such as the need for additional sensors or some kind of digital filter. Also, a control loop is added to the system and the design and analysis of the overall control system become complicated [18–20]. The delay-based inherent damping method is also introduced, which does not need any extra measurements or digital filters and stability of the single-loop control system is ensured at certain ranges of the resonance frequency [21–23]. While damping methods use either a real or a virtual resistor,

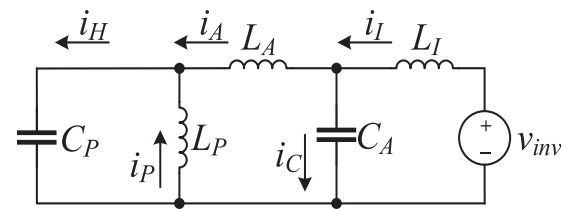


FIGURE 3 Equivalent circuit of Figure 1 with grid shorted and load opened.

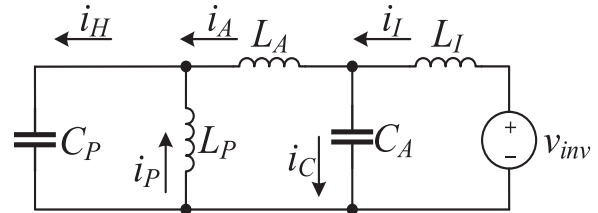


FIGURE 4 Equivalent circuit of Figure 2b.

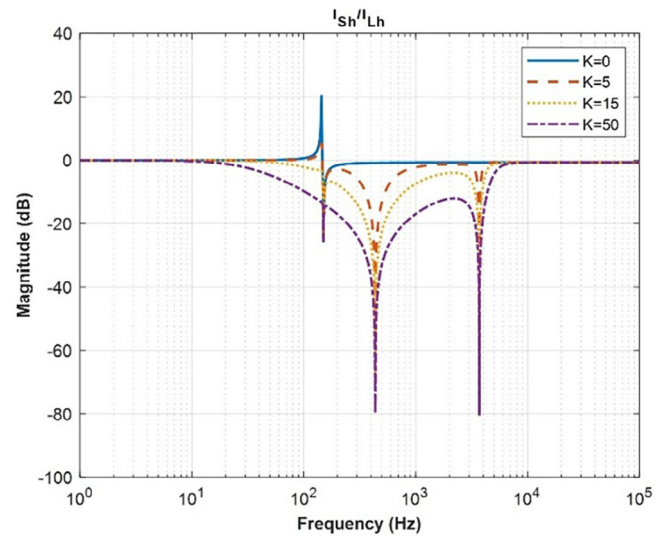


FIGURE 5 HAPF filtering characteristics for different values of K (amplitude diagram).

in the delay-based method, the resonance frequency is carefully selected such that adequate stability margins are obtained for the single-loop control with a certain delay presented in the loop. The effect of the grid impedance when determining the resonance frequency and stability should be considered in this technique.

Reference current generation (RCG) of the APF has a crucial role in the proper operation of the HAPF. Many RCGs are available in the literature that can be categorized into time-domain and frequency-domain techniques. The time-domain RCG schemes include the instantaneous active and reactive power theory (PQ theory), synchronous reference frame (SRF) method and notch filter.

This paper proposes grid voltage sensorless control of an LCL-filtered LC-tuned HAPF structure, shown in Figure 1.

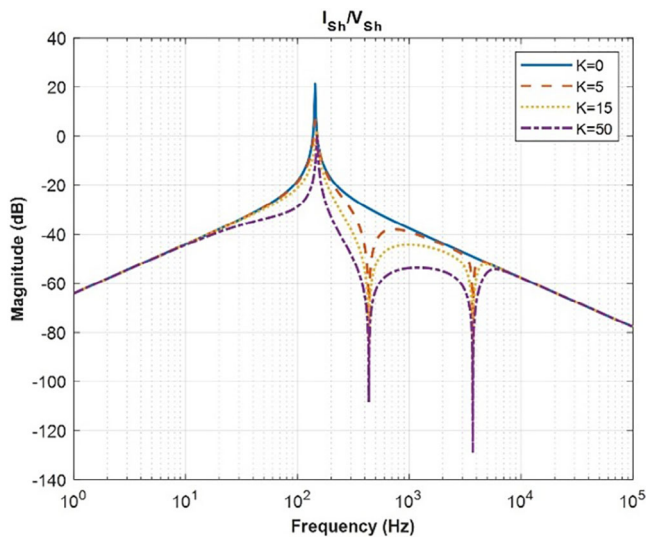


FIGURE 6 HAPF damping characteristics for different values of K (amplitude diagram).

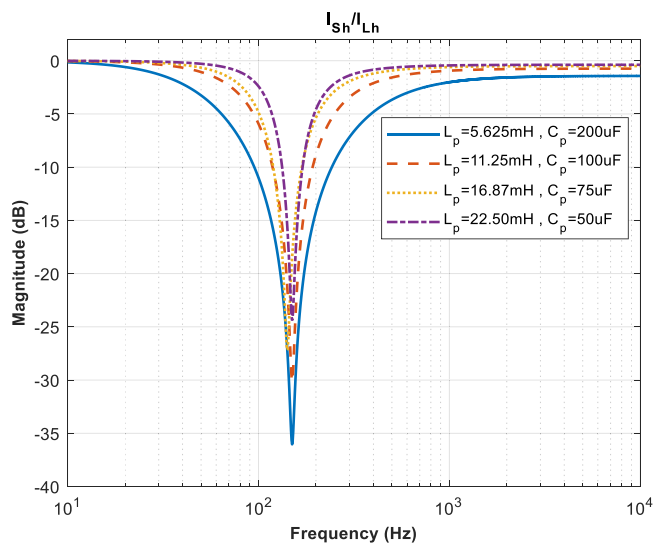


FIGURE 7 PPF compensation characteristics for different values of capacitor C_p and inductor L_p (amplitude diagram).

The simple L-filtered LC-tuned HAPF is already presented in [24–26], which suffers from a large inverter-side inductor and the works lack an exact system modelling and filtering characteristics analysis. In the proposed structure here, the power electronic converter is connected in parallel with the inductance of the passive filter and a high-order LCL filter is used for switching noise attenuation. This configuration considerably reduces the converter current and voltage compared to the conventional HAPFs. The high-order filtering system is modelled and its filtering characteristics are well studied. All parameters are designed based on a simple and step-by-step procedure in the frequency domain. The reference current generation and grid sensorless voltage control are then proposed. The contributions of the paper can be summarized as:

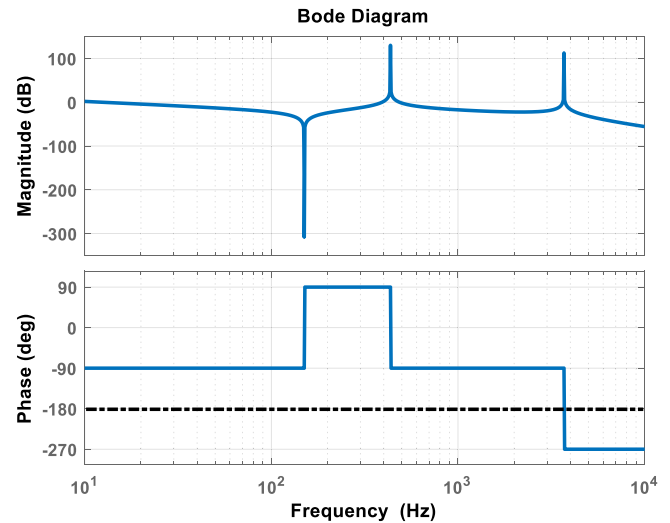


FIGURE 8 Bode diagram of $Y_A(s)$.

TABLE 1 System parameters.

Parameter	Symbol	Value
Grid voltage (RMS)	V_{PCC}	230 V_{rms}
Grid frequency	f	50 Hz
Converter nominal power	S_{rated}	400 VA
DC-link voltage	V_{dc}	150 V
PPF capacitor	C_p	100 μ F
PPF inductor	L_p	11.2 mH
LCL grid-side inductor	L_A	0.75 mH
LCL grid-side inductor	L_I	0.75 mH
LCL capacitor	C_A	5 μ F
Switching/sampling frequency	f_{sw}/f_s	10/20 kHz

- proposing an improved structure of a single-phase shunt hybrid active power filter (HAPF);
- exact modelling of the proposed high-order system and calculating its filtering characteristics;
- straightforward and stable parameters design of the proposed high-order system;
- designing a stable digital current controller;
- replacing the voltage sensor with an estimator.

The paper is organized as follows: Section 2 describes the model of the proposed single-phase shunt HAPF and its filtering characteristics. Section 3 explains the parameters design. Section 4 illustrates the RCG and the detailed design of the grid voltage sensorless control system. Experimental results on a real prototype system are reported in Section 5 and Section 6 concludes the paper.

2 | SYSTEM MODELLING AND FILTERING CHARACTERISTICS

Figure 1 shows the LCL-filtered LC-tuned single-phase shunt HAPF from which one can write:

$$\begin{cases} i_S = i_L - i_H \\ i_A = i_H - i_P \\ i_I = i_A + i_C \end{cases} \quad (1)$$

$$Y_H(s) = \frac{i_H(s)}{v_{inv}(s)} = \frac{L_p C_p s^2}{L_l L_A L_p C_A C_p s^5 + ((L_l + L_A)L_p C_p + L_l(L_A + L_p)C_A) s^3 + (L_l + L_A + L_p)s} \quad (2)$$

$$Y_A(s) = \frac{i_A(s)}{v_{inv}(s)} = \frac{L_p C_p s^2 + 1}{L_l L_A L_p C_A C_p s^5 + ((L_l + L_A)L_p C_p + L_l(L_A + L_p)C_A) s^3 + (L_l + L_A + L_p)s} \quad (3)$$

$$Y_I(s) = \frac{i_I(s)}{v_{inv}(s)} = \frac{L_A L_p C_A C_p s^4 + ((L_A + L_p)C_A + L_p C_p) s^2 + 1}{L_l L_A L_p C_A C_p s^5 + ((L_l + L_A)L_p C_p + L_l(L_A + L_p)C_A) s^3 + (L_l + L_A + L_p)s} \quad (4)$$

where i_S , i_L , i_H , i_P , i_A , i_C , and i_I are the grid, load, HAPF injected, PPF inductor, APF injected, LCL capacitor and single-phase output inverter current, respectively. The equivalent circuits for the fundamental and harmonic components are shown in Figure 2, where the single-phase inverter is assumed as a voltage source proportional to the source harmonic currents as (2) and the load is considered as an ideal current source (I_L) [27].

$$v_{inv}(s) = K \cdot i_{Sb}(s) \quad (5)$$

Also, to obtain the transfer functions in the Laplace domain, the grid is short-circuited and the load is opened. Figure 3 shows the result. Accordingly, the transfer functions from the inverter output voltage to the HAPF, APF, and inverter currents are calculated as (3)–(5). From (2)–(4), the equations for the compensation currents are obtained as (6).

$$\begin{cases} i_H(s) = KY_H(s) \cdot i_{Sb}(s) \\ i_A(s) = KY_A(s) \cdot i_{Sb}(s) \end{cases} \quad (6)$$

According to Figure 2b and using (2), the KVL equation in the left loop is:

$$v_{Sb}(s) = Z_S(s)i_{Sb}(s) - Z_{C_p}(s)i_{Hb}(s) - Z_{L_p}(s)(i_{Hb}(s) - i_{Ab}(s)) \quad (7)$$

where Z_{C_p} and Z_{L_p} are the impedance of the PPF capacitor and inductor, respectively. By substitution of HAPF and APF injected currents (1) and (6) into (7), the HAPF filtering characteristic is obtained as:

$$i_{Sb}(s) = \frac{1}{Z_S(s) + Z_p(s) + KZ_{L_p}(s)Y_A(s)} (Z_p(s)i_{Lb}(s) + v_{Sb}(s)) \quad (8)$$

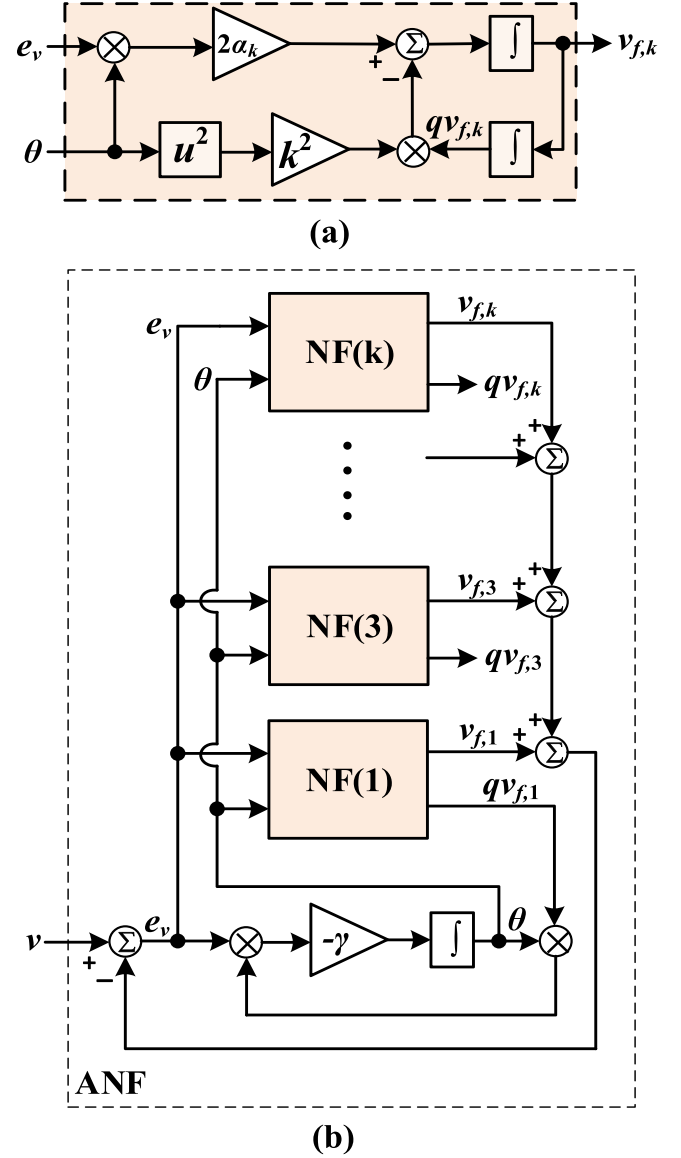


FIGURE 9 (a) Notch filter (NF) block and (b) adaptive notch filter (ANF) structure [28].

where $Z_p = (Z_{C_p} + Z_{L_p})$. As can be seen in (8), the term $KZ_{L_p}(s)Y_A(s)$ represents an equivalent impedance in series with the source in the PPF equivalent circuit replacing the APF. Therefore, the attenuation effect of the compensation impedance, $Z_{Comp} = KZ_{L_p}Y_A$, on different harmonics should be analysed. The compensation impedance can be obtained as (9).

Figure 4 shows the compensation impedance in the circuit. As can be seen, when the APF is not connected to the system ($K = 0$), the equivalent circuit of a single-tuned PPF is obtained. In this condition, when the grid impedance is much smaller than Z_p , the desired filtering characteristics cannot be achieved. In addition, the parallel harmonic resonance between L_S and Z_p may occur in a specific frequency that contributes to the harmonic amplification phenomena. However, when the APF is connected, it helps the PPF to sink the harmonic components

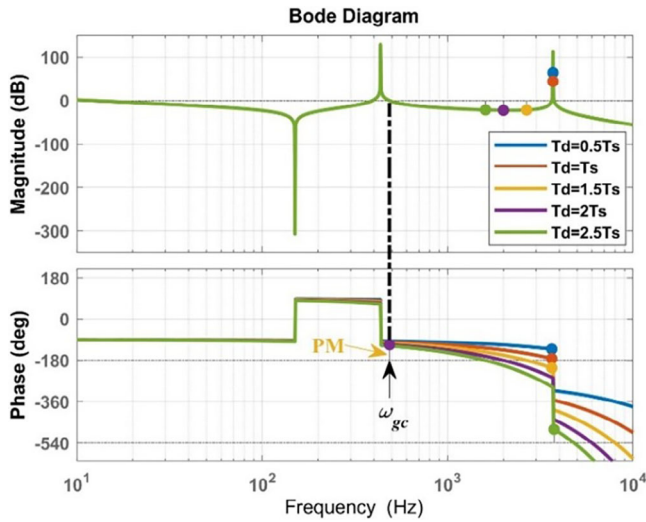


FIGURE 10 Bode diagram of open-loop current control system for different values of T_d ($K_p = 1$).

of load current, I_{Lb} , much more effectively and prevent them from passing through the source. Furthermore, the APF dampens any possible resonances. Figure 5 shows the HAPF filtering characteristics for different values of K . When the APF is not connected ($K = 0$), the harmonic amplification occurs in the frequency range of 100–200 Hz. When the APF is connected and $K > 5$, no harmonic amplification occurs and harmonic damping increases by increasing K . In addition to one notch, corresponding to the PPF tuned frequency of 150 Hz, two other notches in the amplitude diagram are evident, which are related to the LCL filter parameters and its parallel combination with the PPF inductor. It can be readily shown that these two resonances occur at (10).

As can be seen, these two frequencies depend on all HAPF parameters and are very far from each other. The damping characteristic of the HAPF for the source harmonic current is affected by the source harmonic voltage (ignoring the load) and is shown in Figure 6. The damping characteristic is calculated by replacing $i_{Lb} = 0$ in (8). When $K = 0$, the source voltage harmonics cause amplification of source current harmonics from the series resonance. By increasing K , these series resonances caused by the source voltage harmonics are well damped. In Figure 6, two notches can be seen, which are related to the LCL filter.

3 | HAPF PARAMETER DESIGN

In this section, a straightforward procedure to design the HAPF parameters is proposed. First, PPF parameters are calculated according to the required reactive power and the dominant load harmonic to be compensated. Then, the LCL filter parameters are designed according to practical considerations and stability criteria. Accordingly, by effectively employing the inherent delay-based damping the need for passive or active damping is relieved, reducing the losses and the cost.

3.1 | LC-tuned filter parameter design

To design the LC-tuned PPF, several criteria should be considered. The PPF impedance should be as low as possible to reach a good filtering characteristic and reduce the required APF DC-link voltage. The filtering characteristics of the LC-tuned filter for different values of filter inductor and capacitor are compared in Figure 7. Accordingly, the capacitor value should be as high as possible while the inductor value is low to obtain the best filtering performance. Yet, the high capacitance contributes to a high capacitive reactive current through the filter. Also, the low inductance causes the rise of current ripples. Therefore, a tradeoff should be reached. The design of these parameters must be done according to the nonlinear load characteristics and compensation requirements. The capacitor C_p is mainly for load reactive power compensation and the series connection of C_p and L_p is used for selective compensation of the major load harmonic of concern. These parameters are calculated from (11) and (12) where n is the order of PPF tuned harmonic, ω_1 is the fundamental angular frequency, V_S is the RMS value of grid voltage and Q_L is the required load reactive power.

$$C_p = \left(1 - \frac{1}{n^2}\right) \frac{Q_L}{\omega_1 V_S^2} \quad (11)$$

$$L_p = \frac{1}{n^2 \omega_1^2 C_p} \quad (12)$$

$$Z_{Comp}(s) = \frac{KL_p s (L_p C_p s^2 + 1)}{L_l L_A L_p C_A C_p s^5 + ((L_l + L_A)L_p C_p + L_l(L_A + L_p)C_A) s^3 + (L_l + L_A + L_p)s} \quad (9)$$

$$\omega_{res,1,2} = \sqrt{\frac{L_l + L_A}{2L_l L_A C_A} + \frac{L_A + L_p}{2L_A L_p C_p}} \pm \sqrt{\frac{((L_l + L_A)L_p C_p - (L_A + L_p)L_l C_A)^2 + 4L_l^2 L_p^2 C_A C_p}{2L_l L_A L_p C_A C_p}} \quad (10)$$

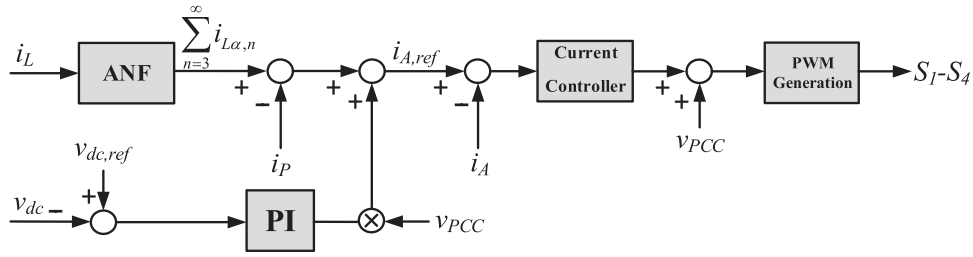


FIGURE 11 Proposed overall control system block diagram.

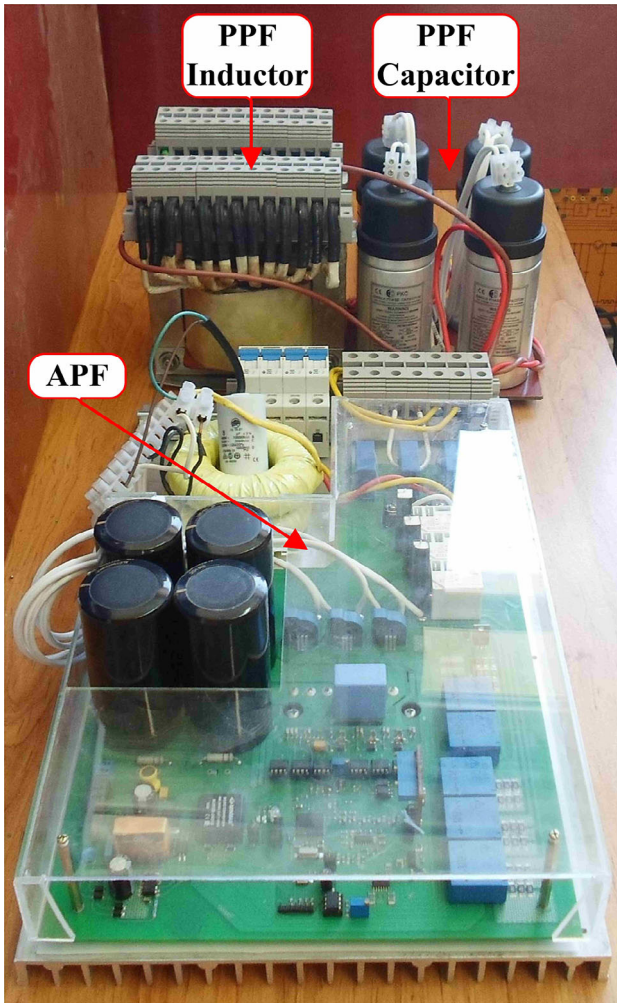


FIGURE 12 Experimental setup.

Here, $n = 3$, $V_s = 230 \text{ V}_{\text{rms}}$, and $Q_L = 2 \text{ kVAR}$. So, the capacitor value is calculated as $107 \mu\text{F}$ from (11) and the standard value of $C_p = 100 \mu\text{F}$ is selected. The PPF inductor is then calculated from (12) as $L_p = 11.25 \text{ mH}$.

3.2 | Practical constraints for LCL filter

Inverter current ripple, grid current harmonics, and capacitor reactive power are three of the most important practical

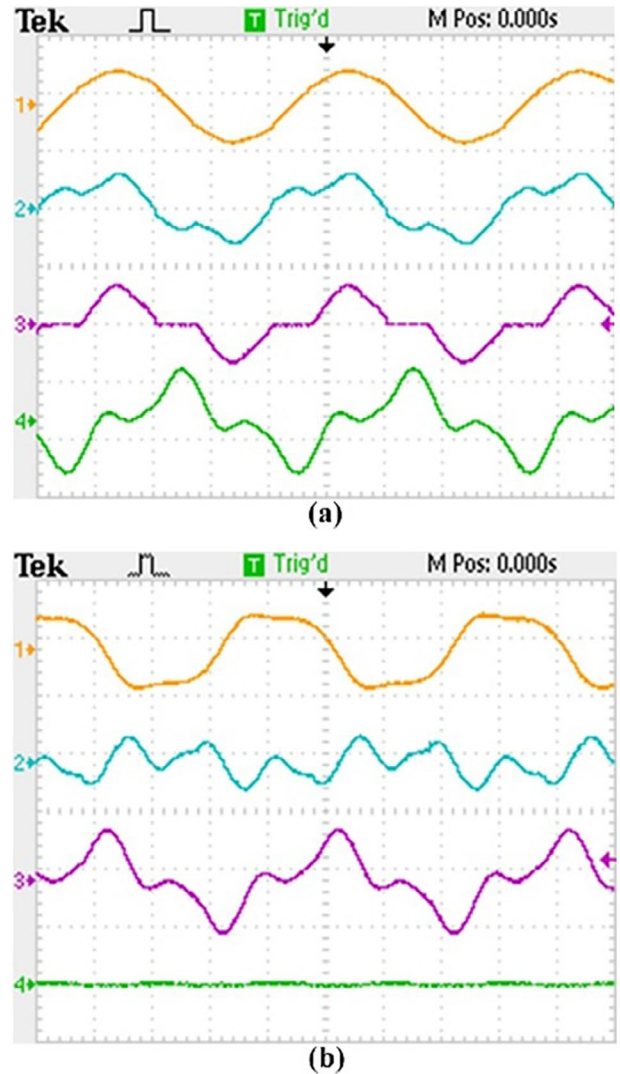
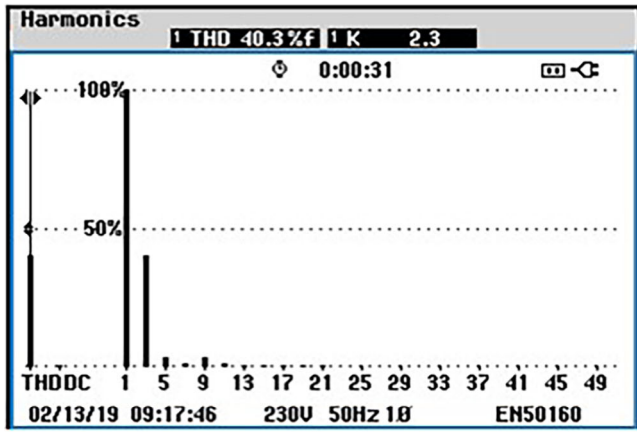


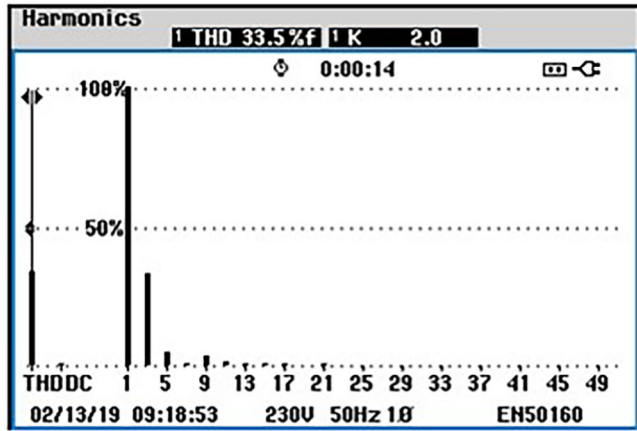
FIGURE 13 Experimental steady-state performance of HAPF when only PPF is connected to PCC: (a) grid voltage (500 V/div), grid current (50 A/div), load current (50 A/div) and HAPF injected current (20 A/div) and (b) PPF capacitor voltage (500 V/div), PPF inductor voltage (200 V/div), PPF inductor current (20 A/div) and APF injected current (10 A/div).

constraints that must be taken into consideration while designing any high-order switching noise smoothing filter [22]:

- The reactive power generated by the capacitor must be limited to a percentage (x_1) of nominal inverter power,



(a)



(b)

FIGURE 14 Experimental steady-state performance of HAPF when only PPF is connected to PCC: (a) load and (b) grid current harmonic spectrums.

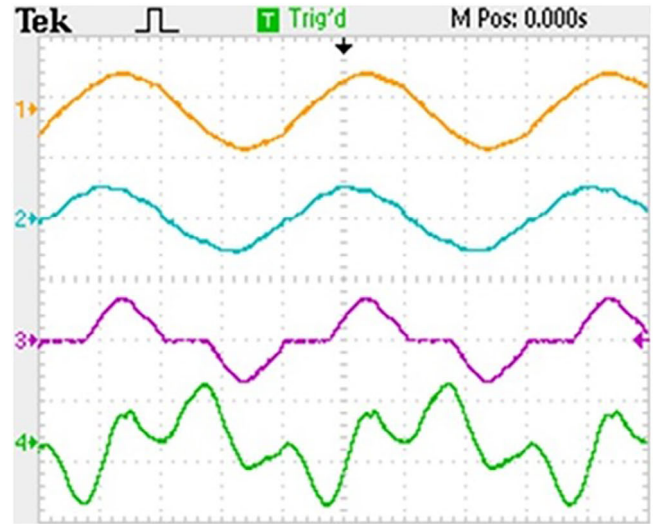
$$C_A \leq \frac{x_1 S_{rated}}{\omega_1 V_{L_p}^2} \quad (13)$$

where S_{rated} is the nominal inverter power and V_{L_p} is the RMS voltage across the PPF inductor. Usually, x_1 is selected in the range of 2.5–5%.

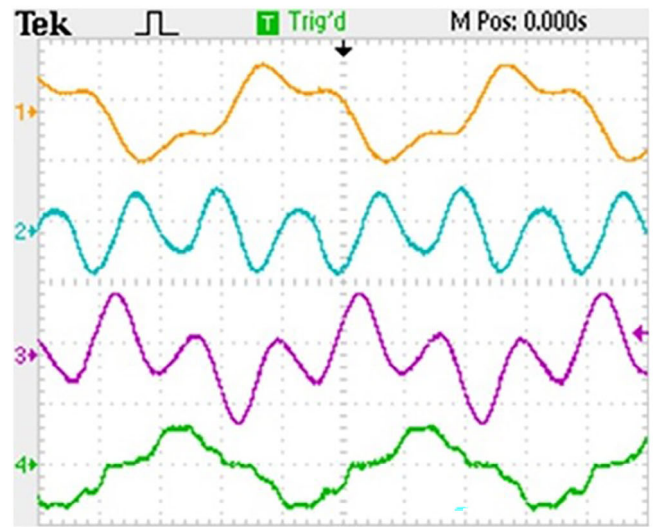
- To limit the semiconductor current rating and core and winding losses, the inverter ripple current is limited to a percentage (x_2) of the nominal peak current ($I_{P,rated}$). Usually, x_2 is selected in the range of 15–40%. The inverter current ripple mainly depends on the inverter-side inductor and is calculated as

$$\Delta i_{I,max} = \frac{V_{dc} T_S}{8L_I} \leq x_2 I_{P,rated} \quad (14)$$

where V_{dc} , T_S , and L_I are the DC-link voltage, the sampling period and the inverter-side inductor. The switching harmonic components must be limited according to relevant standards, such as IEEE 519 which limits harmonic currents greater than 35–0.3% of the nominal current. With the PWM modulation, the dominant harmonics lie around the first switching sideband.



(a)



(b)

FIGURE 15 Experimental steady-state performance of HAPF when PPF and APF are connected to PCC: (a) grid voltage (500 V/div), grid current (50 A/div), load current (50 A/div) and HAPF injected current (20 A/div) and (b) PPF capacitor voltage (500 V/div), PPF inductor voltage (200 V/div), PPF inductor current (20 A/div) and APF injected current (10 A/div).

So, the constraint can be written as

$$i_{A, sb1, max} = |Y_A(j\omega)|_{\omega \gg \omega_{res}} \times V_{sb1, max} \leq x_3 I_{P, rated} \quad (15)$$

where $V_{sb1, max}$ is the maximum of voltage harmonic components at the first sideband and $x_3 = 0.3\%$. Also, the transfer function $Y_A(s)$ should be calculated at high frequencies from (4) as:

$$Y_{A, HF}(s) = |Y_A(j\omega)|_{\omega \gg \omega_{res}} = \frac{1}{L_I L_A C_A \omega^3} \quad (16)$$

- Because harmonic compensation is the final goal of the HAPF structure, control bandwidth should be adequately beyond the highest harmonic component to be compensated.

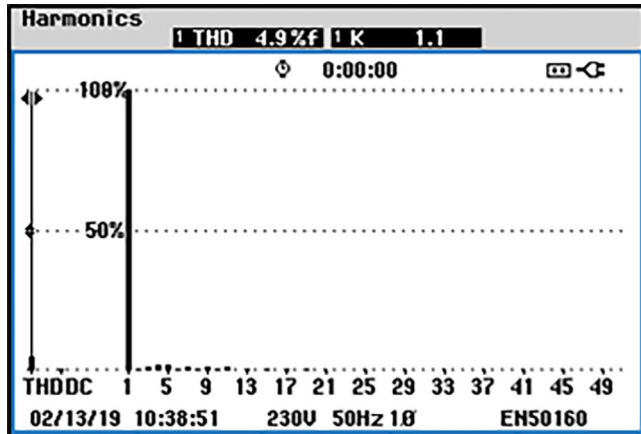


FIGURE 16 Experimental steady-state performance of HAPF when PPF and APF are connected to PCC: grid current harmonic spectrum.

Also, the resonance must not occur within the harmonic compensation region. Therefore:

$$\omega_{res} \geq n_{max} \omega_1 \quad (17)$$

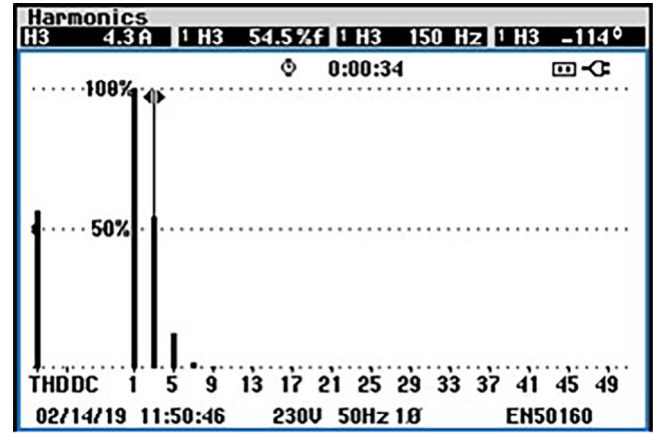
where n_{max} is the maximum harmonic order to be compensated. Here, $n_{max} = 25$ is considered and the resonance frequency calculated from (10) must be higher than 7854 rad/s.

3.3 | Stability constraints for LCL filter

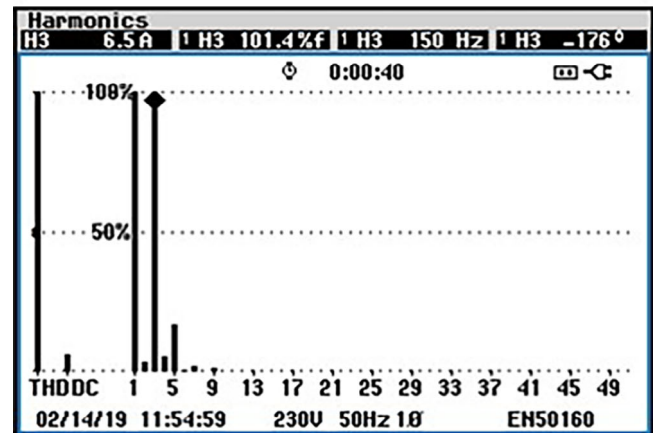
Figure 8 shows the Bode diagram of $Y_A(s)$. As can be observed, the phase diagram starts at -90° , then jumps to $+180^\circ$ at the trap frequency (tuned frequency of the PPF), falls to -180° at the first resonance frequency and finally falls to -180° again at the second resonance frequency and remained at -270° . Also, it is observed that the system without the controller and the digital delay is unstable; because the magnitude characteristic is greater than zero when the phase crosses -180° at the second resonance frequency. So, the first resonance frequency does not affect the system stability in this condition. So, it must be guaranteed that the phase lies between -180° and -540° just before the second resonance. It is proven that in the presence of digital implementation delay, T_d , the current control system will be stable if the second resonance frequency lies in the range defined by $f_S/6 < f_{res} < f_S/2$ (where $f_S/6$ is the critical frequency of the filter and is defined as f_{min} during the following design procedure) that results in (18) [21–23].

$$2\pi \underbrace{\frac{f_S}{6}}_{f_{min}} \leq \omega_{res,2} \leq 2\pi \underbrace{\frac{f_S}{2}}_{f_{max}} \quad (18)$$

These constraints and the resonance frequencies are obtained with the assumption that $L_S = 0$. On the other hand, if the grid impedance tends to infinity, the series connection of the grid impedance and the PPF capacitor tends to infinity. So, the parallel connection of them with the PPF inductor simplifies



(a)



(b)

FIGURE 17 Experimental steady-state performance of HAPF: PPF current harmonic spectrum (a) without and (b) with APF in circuit.

to the PPF inductor itself. Therefore, under the infinite grid impedance condition, the second resonance frequency must satisfy the following constraint:

$$\omega_{res2,min} = \frac{L_I + L_A + L_P}{L_I(L_A + L_P)C_A} \geq (2\pi f_{min})^2 \quad (19)$$

Therefore, to ensure that the resonance frequencies are within the stable range, constraint (19) and the right-hand side of (18) must be satisfied simultaneously.

3.4 | LCL filter parameter design

With the sets of practical and stability constraints for the LCL filter, now one can design a stable LCL filter with adequate attenuation performance. To design the filter, first x_1 , x_2 , and x_3 should be decided. Then, LCL filter parameters can be calculated following a straightforward procedure, described below.

- Capacitor value first should meet the constraint (13) according to the practical constraints. By substituting (14) into (19),

TABLE 2 Performance comparison.

	Load current THD	Grid current THD	Inverter DC-link voltage	APF RMS current	Inverter power
PPF (3rd tuned)	41%	33.5%	—	—	—
APF	41%	2.3%	400 V	6.5 A _{rms}	1800 VA
HAPF of [15]	41%	2.4%	150 V	9.75 A _{rms}	740 VA
Proposed structure	41%	4%	150 V	3.10 A _{rms}	310 VA

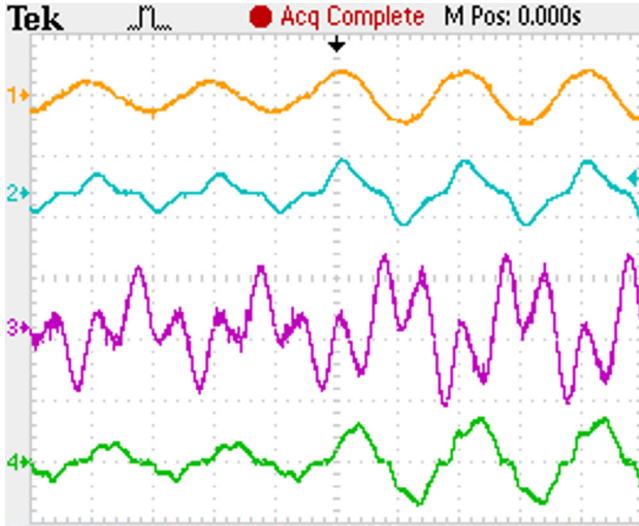


FIGURE 18 Experimental transient performance of HAPF in response to load increase when PPF and APF are connected to PCC: (a) grid current (100 A/div), load current (100 A/div), PPF inductor current (20 A/div) and APF injected current (20 A/div).

the stability constraint for the capacitor is obtained as:

$$C_A \leq \frac{V_{dc} T_S + 8x_2 I_{P,rated} (L_A + L_P)}{V_{dc} T_S (L_A + L_P) (2\pi f_{min})^2} \quad (20)$$

which readily simplifies to:

$$C_A \leq \frac{8x_2 I_{P,rated}}{V_{dc} T_S (2\pi f_{min})^2} \quad (21)$$

The minimum value obtained from (13) and (21) will be chosen for the capacitor.

- After calculating the capacitor, the inverter-side inductor is calculated as:

$$L_I = \frac{1}{C_A (2\pi f_{min})^2} \quad (22)$$

It is worth noting that the allowed ripple limit for the inverter current is considered for the capacitor design in the previous step, and then the calculated inductance satisfies the constraint (14).

- Finally, L_A has to be chosen in a way that in addition to appropriate attenuation of switching harmonics, system stability is guaranteed. To meet the IEEE standard,

Equation (15) can be rewritten as:

$$L_A \geq \frac{V_{sb1,max}}{L_I C_A (2\pi f_s)^3 x_3 I_{P,rated}} \quad (23)$$

After calculating C_A , L_I , and L_A , these parameters must satisfy the constraints (18) and (19). If these conditions are not met, the value of the capacitor should be decreased and the design procedure should be repeated. Here, $x_1 = 5\%$, $x_2 = 20\%$, and $x_3 = 0.2\%$. The achieved LCL filter parameters are shown in Table 1.

4 | RCG AND GRID SENSORLESS VOLTAGE CONTROL SYSTEM DESIGN

4.1 | RCG

The nonlinear load current can be decomposed into active, reactive and harmonic currents. The final goal of the HAPF is to compensate the harmonic components of the load current resulting in a pure sinusoidal waveform drawn from the grid. Many harmonic extraction methods in the time domain are already available, such as the high-pass or the low-pass filters to extract the harmonic power in the natural reference frame or to extract the fundamental current in the synchronous reference frame, notch filter (NF) etc. [6–15, 24–26]. The high dependency of harmonic extraction performance on the cut-off frequency of low-pass and high-pass filters leads to a weak dynamic performance of these methods. Also, the NF method is very sensitive to frequency changes. To overcome this problem, the adaptive notch filter (ANF) method is introduced, in which the centre frequency adaptively changes with the input frequency variations [28–29]. So, the ANF is a simple and effective technique for voltage and current harmonics extraction. Here, the load current harmonics are extracted by using ANF. The ANF structure is shown in Figure 9. As can be seen, each NF block is responsible for the determined harmonic component extraction and a simple method is presented for the input frequency extraction. In this technique, the in-phase harmonic components to be compensated are extracted individually. The sum of these components except the fundamental forms the reference current of the HAPF. With the APF in the circuit, the APF reference current is calculated by subtracting the measured PPF inductor current from the HAPF reference current.

4.2 | Digital control system design

The HAPF control system is based on accurate control of the APF injected current, i_A . Here, a simple proportional controller is utilized and will be shown that successfully provides high quality and exact performance. So, the discrete-time closed-loop transfer function of the APF current can be written as:

$$\frac{i_A(z)}{i_{A,ref}(z)} = \frac{G_C(z)G_{delay}(z)Y_A(z)}{1 + G_C(z)G_{delay}(z)Y_A(z)} \quad (24)$$

where $G_C(z) = K_p$ is the system proportional controller and $G_{delay}(z) = z^{-T_d/T_s}$ is the delay function where T_d represents the total digital control delay caused by the A/D conversion, computations and the PWM modulator and is $1.5T_s$ for a double-updated PWM modulator, and $Y_A(z)$ is the discretized version of $Y_A(s)$. Figure 10 shows the Bode diagrams of the open-loop current control system for different values of T_d , when $K_p = 1$. According to this figure, the control system is stable for $T_d = 1.5T_s$ and the sharp phase change of the second resonance frequency is within -180° and -540° . To tune the proportional gain, the phase margin (PM) is set to the desired value. To do this, first, the phase angle of the open-loop current control system at the gain crossover frequency, ω_{gc} , is calculated as:

$$\begin{aligned} \angle \frac{i_A(z)}{i_{A,ref}(z) - i_A(z)} \Big|_{s=j\omega_{gc}} &= \angle K_p e^{-j\omega_{gc}T_d} Y_A(e^{j\omega_{gc}}) \\ &= -j\omega_{gc}T_d - \frac{\pi}{2} \end{aligned} \quad (25)$$

and by equating this phase angle to $(PM - \pi)$, the crossover frequency is obtained as:

$$\omega_{gc} = \frac{(\pi/2 - PM)}{T_d} \quad (26)$$

To attain the unity loop gain at the crossover frequency, the proportional gain then must be as:

$$K_p = \frac{\omega_{gc} \left(L_l L_A L_p C_A C_p \omega_{gc}^4 - (L_l + L_A) L_p C_p \omega_{gc}^2 \right)}{1 - L_p C_p \omega_{gc}^2} \quad (27)$$

Here, PM is considered to be 45° and thus, ω_{gc} and K_p are obtained from (26) and (27) as 1667 Hz and 11.9, respectively.

Figure 11 shows the proposed overall control system along with the RCG. As can be seen, to keep the DC-link voltage of the converter in its reference value, a low active power must be injected. For this, the difference between the DC-link voltage of the converter and its reference value is given to a PI controller and its output is multiplied by the grid voltage to be added to the APF reference current. Here, a grid voltage estimation technique is employed to reduce the cost and size of the APF system. This estimation technique uses the measured APF injected current, PPF inductor current and the PPF parameters as input. The equation of the grid voltage estimator at the

point of common coupling (PCC) is presented in (28) and is implemented in the discrete domain as (29).

$$v_{PCC} = -v_{C_p} - v_{L_p} = -\frac{1}{C_p} \int (i_p + i_A) dt - L_p \frac{di_p}{dt} \quad (28)$$

$$\begin{aligned} v_{PCC}[kT_s] &= -v_{C_p}[kT_s] - v_{L_p}[kT_s] \\ \begin{cases} v_{C_p}[kT_s] &= v_{C_p}[(k-1)T_s] + (T_s/C_p) \times (i_p[kT_s] + i_A[kT_s]) \\ v_{L_p}[kT_s] &= (L_p/T_s) \times (i_p[kT_s] - i_p[(k-1)T_s]) \end{cases} \end{aligned} \quad (29)$$

So, the grid voltage is estimated through some simple calculations. To reduce the distortions and noises in the estimated grid voltage, the estimated voltage is fed to an ANF and its fundamental component is then extracted to be fed to the control system. It should be noted that only the first and third components are considered in the ANF structure.

The outputs of the PWM generation block are gating signals for the inverter switches. Also, as can be seen, a feedforward of the grid voltage is added to the control signal to improve disturbance rejection and enhance system dynamics.

5 | EXPERIMENTAL RESULTS

To support the theoretical achievements and confirm the proper steady-state and transient operation of the HAPF a laboratory prototype is built (Figure 12). The system and filter parameters are listed in Table 1. The nonlinear load consists of a single-phase full-bridge diode rectifier feeding a resistor in parallel with a capacitor. The control algorithm is implemented on an STM32F407VGT6 digital signal controller from STMicroelectronics. The waveforms are recorded by Tektronix TPS2014B oscilloscope. Furthermore, the harmonic spectrums are evaluated using a Fluke 435 power quality analyzer. The grid voltage has a total harmonic distortion (THD) equal to 4.44%. Figure 13a shows the steady-state grid voltage, grid current, load current, and HAPF injected current when only the PPF is connected to the PCC and the APF is disconnected. The harmonic spectrums of the load and the grid currents are shown in Figures 14a and 14b, respectively. The load current THD is about 41% and the grid current THD decreases to 33.5%, which shows a slight reduction. Figure 13b demonstrates the steady-state PPF capacitor voltage, PPF inductor voltage, PPF inductor current, and APF current (zero). In this situation, the RMS currents of the load, grid and PPF are 17.17, 18.31, and 9.15 A, respectively. When the APF is operating, the source current THD decreases to 4.9% as waveforms are depicted in Figure 15 where a sinusoidal grid current is evident. The harmonic spectrum of the grid current is shown in Figure 16. As can be seen, the grid current meets the standard limit of 5% and the main harmonic orders (the third, fifth, seventh, and ninth) are well limited. Figure 17 shows the PPF inductor current harmonic spectrum, before and after the APF connection. According to the figure, when the APF is not in operation, the PPF current contains major fifth and seventh harmonics. When

the APF is connected, only the third harmonic goes through the PPF and the APF injects a small third-order component and all the other harmonic components. So, the PPF current is reduced in this condition as the RMS currents of the grid, PPF inductor and APF are 17.58, 9.16, and 3.10 A, respectively. Evidently, with a small APF current, a perfect harmonic compensation is possible and the RMS current of the grid also decreases.

Figure 18 shows the transient response of the APF system to a step increase in the load current. The filter current tracks its reference. Proper operation of both RCG and current controller ensures the grid current maintains a sinusoidal waveform after a sudden boost in the load current.

To demonstrate the superiority of the proposed HAPF structure over the conventional ones, the proposed structure is compared with the PPF, APF, and conventional HAPF of [15] through extensive simulations and the results are summarized in Table 2. The PPF and APF in the HAPF structure of [15] are in series and an LCL filter is employed at the inverter output. The non-linear load of Figures 13 and 14 is connected to the PCC and the filtering performance for four structures is compared in Table 2. As can be seen, the grid current THD of the proposed structure is higher than the conventional HAPF structure and pure APF, however, it is still within the standard range. The main difference between the structures is the APF injected current (RMS) and the APF power. The converter RMS current of the pure APF is about double the proposed method and for conventional HAPF structure is about triple the proposed structure, which demands higher rating, loss, and cost for the inverter circuit.

6 | CONCLUSION

This paper proposes grid voltage sensorless control of an LCL-filtered LC-tuned single-phase shunt HAPF. With the proposed structure, the APF power requirements and costs are greatly reduced. Exact modelling of the high-order system and its filtering characteristics is done, and a straightforward design of the filter parameters is presented. The LCL filter design incorporates stability constraints to achieve a stable operation without the need for an extra damping method. An efficient RCG technique is employed and a simple proportional controller is utilized to track the filter reference current. The stability of the current control system is studied here. To reduce the cost and size of the APF system even more, a grid voltage estimation technique is proposed. The experimental results on a real prototype are provided to demonstrate the validity of the theoretical results and effectiveness of the suggested structure in both steady-state and transient situations. Furthermore, a comparison between the proposed HAPF structure and a successful conventional technique is performed, and the results confirm how the inverter ratings are reduced by more than half while the overall compensation performance still satisfies the standard requirements.

AUTHOR CONTRIBUTIONS

Mohammad-Sadegh Karbasforooshan: Formal analysis; investigation; methodology; software; validation; visualization; writing—Original draft preparation. **Mohammad Monfared:** Conceptualization; formal analysis; investigation; methodology; project administration; project administration; project administration

CONFLICT OF INTEREST STATEMENT

The authors declare no conflicts of interest.

FUNDING INFORMATION

The authors received no specific funding for this work.

DATA AVAILABILITY STATEMENT

The data that support the findings of this study are available from the corresponding author, upon reasonable request.

ORCID

Mohammad Monfared  <https://orcid.org/0000-0002-8987-0883>

REFERENCES

- Manai, L., Hakiri, D., Besbes, M.: Backstepping control of flying capacitor multilevel inverter-based active power filter. *IET Power Electron.* 13(19), 4610–4624 (2021)
- Zhang, Z., Yi, H., Zhuo, F., Li, Y.-G., Jiang, X.: Harmonic oscillation analysis and stabilization method comparison of shunt active power filter in full compensation mode. *IET Power Electron.* (2023)
- Karbasforooshan, M.-S., Monfared, M.: Multi-resonant indirect digital current control technique for single-phase shunt active power filters. *Electr. Power Compon. Syst.* 47(13), 1196–1202 (2019)
- Alhasheem, M., Mattavelli, P., Davari, P.: Harmonics mitigation and non-ideal voltage compensation utilising active power filter based on predictive current control. *IET Power Electron.* 13(13), 2782–2793 (2020)
- Karbasforooshan, M.-S., Monfared, M.: An improved reference current generation and digital deadbeat controller for single-phase shunt active power filters. *IEEE Trans. Power Delivery* 35(6), 2663–2671 (2020)
- Asadi, M., Jalilian, A.: Control of hybrid active power filter based on switching function coefficients. *Electr. Power Compon. Syst.* 43(13), 1498–1508 (2015)
- Saha, T.K., Krause, O., Cao, Y., Liu, F., Li, Y.: Hybrid inductive and active filtering method for damping harmonic resonance in distribution network with non-linear loads. *IET Power Electron.* 8(9), 1616–1624 (2015)
- Durna, E.: Adaptive fuzzy hysteresis band current control for reducing switching losses of hybrid active power filter. *IET Power Electron.* 11(5), 937–944 (2018)
- Rahmani, S., Hamadi, A., Al-Haddad, K., Dessaint, L.A.: A combination of shunt hybrid power filter and thyristor-controlled reactor for power quality. *IEEE Trans. Ind. Electron.* 61(5), 2152–2164 (2014)
- Wang, L., Lam, C.-S., Wong, M.-C.: A hybrid-STATCOM with wide compensation range and low DC-link voltage. *IEEE Trans. Ind. Electron.* 63(6), 3333–3343 (2016)
- Wang, L., Lam, C.-S., Wong, M.-C.: Modeling and parameter design of thyristor-controlled LC-coupled hybrid active power filter (TCLC-HAPF) for unbalanced compensation. *IEEE Trans. Ind. Electron.* 64(3), 1827–1840 (2017)
- Verma, V., Singh, B.: Design and implementation of a current-controlled parallel hybrid power filter. *IEEE Trans. Ind. Appl.* 45(5), 1910–1917 (2009)
- Gonzatti, R.B., Ferreira, S.C., da Silva, C.H., Pereira, R.R., Borges da Silva, L.E., Lambert-Torres, G.: Smart impedance: A new way to look at hybrid filters. *IEEE Trans. Smart Grid* 7(2), 837–846 (2016)

14. Han, Y., Xu, L., Khan, M.M., Chen, C., Yao, G., Zhou, L.-D.: Robust deadbeat control scheme for a hybrid APF with resetting filter and ADALINE-based harmonic estimation algorithm. *IEEE Trans. Ind. Electron.* 58(9), 3893–3904 (2011)
15. Mishra, S., Ray, P.K.: Nonlinear modeling and control of a photovoltaic fed improved hybrid DSTATCOM for power quality improvement. *Int. J. Electr. Power Energy Syst.* 75, 245–254 (2016)
16. Peña-Alzola, R., Liserre, M., Blaabjerg, F., Sebastián, R., Dannehl, J., Fuchs, F.W.: Analysis of the passive damping losses in LCL-filter-based grid converters. *IEEE Trans. Power Electron.* 28(6), 2642–2646 (2013)
17. Beres, R.N., Wang, X., Blaabjerg, F., Liserre, M., Bak, C.L.: Optimal design of high-order passive-damped filters for grid-connected applications. *IEEE Trans. Power Electron.* 31(3), 2083–2098 (2016)
18. Pena-Alzola, R., Liserre, M., Blaabjerg, F., Ordóñez, M., Kerekes, T.: A self-commissioning notch filter for active damping in a three-phase LCL-filter-based grid-tie converter. *IEEE Trans. Power Electron.* 29(12), 6754–6761 (2014)
19. Parker, S.G., McGrath, B.P., Holmes, D.G.: Regions of active damping control for LCL filters. *IEEE Trans. Ind. Appl.* 50(1), 424–432 (2014)
20. Xin, Z., Loh, P.C., Wang, X., Blaabjerg, F., Tang, Y.: Highly accurate derivatives for LCL-filtered grid converter with capacitor voltage active damping. *IEEE Trans. Power Electron.* 31(5), 3612–3625 (2016)
21. Wang, J., Yan, J.D., Jiang, L., Zou, J.: Delay-dependent stability of single-loop controlled grid-connected inverters with LCL filters. *IEEE Trans. Power Electron.* 31(1), 743–757 (2016)
22. Sanatkar-Chayjani, M., Monfared, M.: Design of LCL and LLCL filters for single-phase grid connected converters. *IET Power Electron.* 9(9), 1971–1978 (2016)
23. Sanatkar-Chayjani, M., Monfared, M.: Stability analysis and robust design of LCL with multituned traps filter for grid-connected converters. *IEEE Trans. Ind. Electron.* 63(11), 6823–6834 (2016)
24. Wu, J., Jou, H., Wu, K., Hsiao, H.: Three-phase four-wire hybrid power filter using a smaller power converter. *Electr. Power Syst. Res.* 87, 13–21 (2012)
25. Wu, J.-C., Jou, H.-L., Hsiao, H.-H., Xiao, S.-T.: A new hybrid power conditioner for suppressing harmonics and neutral-line current in three-phase four-wire distribution power systems. *IEEE Trans. Power Delivery* 29(4), 1525–1532 (2014)
26. Deng, Y., Tong, X., Jia, H.: A bidirectional control principle of active tuned hybrid power filter based on the active reactor using active techniques. *IEEE Trans. Ind. Inf.* 11(1), 141–154 (2015)
27. Srianthumrong, S., Akagi, H.: A medium-voltage transformerless AC/DC power conversion system consisting of a diode rectifier and a shunt hybrid filter. *IEEE Trans. Ind. Appl.* 39(3), 874–882 (2003)
28. Chilipi, R.S.R., Al Sayari, N., Al Hosani, K.H., Beig, A.R.: Adaptive notch filter-based multipurpose control scheme for grid-interfaced three-phase four-wire DG inverter. *IEEE Trans. Ind. Appl.* 53(4), 4015–4027 (2017)
29. Lenka, R.K., Panda, A.K., Patel, R., Guerrero, J.M.: PV integrated multi-functional off-board EV charger with improved grid power quality. *IEEE Trans. Ind. Appl.* 58(5), 5520–5532 (2022)

How to cite this article: Karbasforooshan, M.-S., Monfared, M.: Grid voltage sensorless control of a single-phase shunt hybrid active power filter. *IET Power Electron.* 17, 752–763 (2024).
<https://doi.org/10.1049/pel2.12689>